Critical behaviour and conformal anomaly of the O(n) model on the square lattice

1989 J. Phys. A: Math. Gen. 22 1415

(http://iopscience.iop.org/0305-4470/22/9/028)

J. Phys. A: Math. Gen. **22** (1989) 1415-1438. Printed in the UK

Critical behaviour and conformal anomaly of the O(n) model on the square lattice

Henk W J Blöte† and Bernard Nienhuis‡

† Laboratorium voor Technische Natuurkunde, Technische Universiteit Delft, Lorentzweg 1, 2628 CJ Delft, The Netherlands

‡ Instituut Lorentz, Rijksuniversiteit Leiden, Nieuwsteeg 18, 2311 SB Leiden, The Netherlands

Received 22 November 1988

Abstract. Finite-size scaling and transfer-matrix techniques are used to determine the conformal anomaly and critical exponents of O(n) models on the square lattice. These calculations were performed on five branches of critical points parametrised by n. The results for two of the branches agree with the known universal properties of the O(n) model as derived for the honeycomb lattice. Finite-size convergence is poor for most of the third branch, so that in this case the classification in terms of known models is uncertain. Our data show that the fourth branch can be interpreted in terms of a combination of a low-temperature O(n) and a critical Ising model. Finally, the numerical results for the O(n) model on the remaining branch agree accurately with the known results for the low-temperature O($n+1$) model. We prove this equivalence by means of an exact mapping.

1. Introduction

The O(n) model was originally defined [1] as a system of n-dimensional vectors (spins) which interact in a rotationally invariant way. For a specific choice of the interactions between the spins, the partition function can be expressed [2] in terms of a loop gas. In this model, n is a continuous variable. The equivalence between the O(n) spin model and the loop gas has made it possible to derive some exact information about the critical O(n) model. In particular for the honeycomb O(n) model, some results were obtained [3, 4] in the range $-2 \leqslant n \leqslant 2$ from a mapping of the loop model onto the Coulomb gas. More recently, Bethe ansatz solutions [5-7] of vertex model representations of the honeycomb loop model have been found. Thus, the asymptotic finite-size dependence of several eigenvalues of the transfer matrix could be determined [6]. Comparison with the theory of conformal invariance [8-10] in critical models yielded the conformal anomaly and several critical dimensions, confirming earlier results [3, 4, 11-13].

Very recently Nienhuis [14] investigated an O(n) model with the n-component spins on the middle of the edges of a square lattice. The Boltzmann weight for each spin configuration is the product over all vertices of the lattice of the local weight

$$Q = 1 + u(s_1 \cdot s_2 + s_2 \cdot s_3 + s_3 \cdot s_4 + s_4 \cdot s_1) + v(s_1 \cdot s_3 + s_2 \cdot s_4) + w[(s_1 \cdot s_2)(s_3 \cdot s_4) + (s_2 \cdot s_3)(s_4 \cdot s_1)] \tag{1.1}$$

where the spins s_1 through s_4 sit on the four edges incident on the vertex and are labelled anticlockwise. Expansion of the partition sum in powers of the coupling constants u, v and w turns the model into a loop gas [2]. The configurations of this

0305-4470/89/091415+24$02.50

loop gas are the graphs $\mathcal{G}$ consisting of non-intersecting closed polygons covering some (or none) of the edges of the square lattice. Each vertex is visited zero, one or two times by these polygons and thus has one of the nine appearances shown in figure 1, and a weight 1, u, v or w accordingly. The partition sum is

$$Z = \sum_{\mathcal{G}} u^{N_u} v^{N_v} w^{N_w} n^{N_l}. \tag{1.2}$$

The exponents denote the number of vertices of the type indicated, and the number of loops. While the configurations of this loop gas can be interpreted as the diagrams in the high-temperature expansion of the O(n) model defined by (1.1), they can also be seen as the low-temperature expansion of a cubic model, of which the n-component spins, sitting on the faces of the lattice, point to the corners of a hypercube [2]. Two spins on adjacent faces may differ in at most one spin component. Weights are associated with configurations around each vertex, and are equal to 1 when all four spins are parallel, u when one spin differs from the other three, v when one pair of adjacent spins differs form the other pair, $2w$ when one pair of diagonally opposed spins differs from the other pair, w when two diagonally opposed spins are equal and the other two are different from the first and from each other, and 0 when all four spins are different. These three interpretations of the same partition sum will be referred to as O(n) model, loop gas and corner-cubic model respectively.

Nienhuis [14] has found a set of critical points of this model. This set can be divided into five curves parametrised by n, which will, for easy reference, be labelled as branch 0 to branch 4. The weights u, v and w for branch 0 are

$$u = w = \tfrac{1}{2} \qquad v = 0. \tag{1.3}$$

The four remaining branches, on which the model turns out to be equivalent to a nineteen-vertex model studied by Izergin and Korepin [15] and others [16], are given by

$$\begin{aligned} w &= \{2-[1-2\sin(\theta/2)][1+2\sin(\theta/2)]^2\}^{-1} \\ u &= \pm 4w \sin(\theta/2)\cos(\pi/4-\theta/4) \\ v &= \pm w[1+2\sin(\theta/2)] \\ n &= -2\cos(2\theta). \end{aligned} \tag{1.4}$$

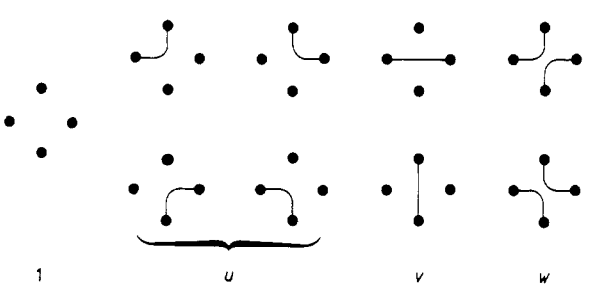

Figure 1. The Boltzmann weights of the nine vertices that occur in the loop model representation of the O(n) model. The points indicate the sites of the n-component spins on the middle of the edges of the simple quadratic lattice. The vertices are divided into four groups. The weights are normalised such that empty vertices have weight one.

The branches are intervals in θ:

$$\frac{\pi}{2} \leqslant \theta \leqslant \pi \qquad \text{branch 1}$$

$$0 \leqslant \theta \leqslant \frac{\pi}{2} \qquad \text{branch 2}$$

$$-\frac{\pi}{2} \leqslant \theta \leqslant 0 \qquad \text{branch 3}$$

$$-\pi \leqslant \theta \leqslant -\frac{\pi}{2} \qquad \text{branch 4.}$$

Since vertices of type u occur an even number of times, the sign of u is irrelevant, and we may choose $u \geqslant 0$ without loss of generality. But the sign of v is of some importance in the case of periodic boundaries: the weight of loops closing over the periodic boundary depends on the sign of v, at least for odd system sizes. However, we expect that such effects become unimportant in the bulk limit and we will restrict ourselves to $v \geqslant 0$ when no mention of the sign is made. The w-type vertices may occur in even as well in odd numbers, irrespective of system sizes and boundary conditions. Therefore, there is no arbitrariness in the sign of w in (1.4).

While the O(n) model has been argued to be critical on these five branches, the classification of the critical behaviour in terms of universality classes remains to be found. In order to tackle this problem, it is very helpful that the theory of conformal invariance has established relations between the finite-size amplitudes of two-dimensional models, and their scaling dimensions. One key result of the theory of conformal invariance [8–10] is that a model can be characterised by the central charge c. This quantity is related to the finite-size dependence of the free energy. For an $L \times \infty$ system with periodic boundaries in the L direction, the free energy f per vertex behaves asymptotically as [10, 13, 17]

$$f(L) \simeq f(\infty) + \pi c/(6L^2) \tag{1.5}$$

and the correlation lengths behave asymptotically linear in the system size:

$$\xi_i^{-1}(L) \simeq 2\pi X_i / L \tag{1.6}$$

where X_i is the scaling dimension and ξ_i the correlation length of the ith operator [18]. Besides, for $c \leqslant 1$, the central charge and the scaling dimensions are related by the Kac formula [8, 9]. Parametrising c by

$$c = 1 - \frac{6}{m(m+1)} \tag{1.7}$$

the scaling dimensions for scalar operators satisfy

$$X_i = 2\Delta(p_i, q_i) \qquad \Delta(p_i, q_i) = \frac{[p_i(m+1) - q_i m]^2 - 1}{4m(m+1)} \tag{1.8}$$

where p_i and q_i are integers that are characteristic for the ith operator.

The finite-size quantities $f(L)$ and $\xi_i(L)$ are related to the eigenvalues $\Lambda_L^{(i)}$ of the transfer matrix as follows:

$$f(L) = L^{-1} \log \Lambda_L^{(0)} \tag{1.9}$$

$$\xi_i^{-1}(L) = \log [\Lambda_L^{(0)} / \Lambda_L^{(i)}] \tag{1.10}$$

where Λ_0 and Λ_i are the leading and the ith eigenvalue. Thus, the central charge and the scaling dimensions can be estimated from the eigenvalues of the transfer matrix as functions of the system size L. Therefore we have constructed a transfer matrix for the loop model; this is explained in § 2. An analysis of the results is presented in § 3. That section also contains some conclusions about the universality classification of the five branches, as far as they are directly indicated by the numerical results. A further discussion of these results is given in § 4.

2. Construction of the transfer matrix

Guided by reasons of computational convenience, we start from the loop representation of the O(n) model. The vertex representation offers an alternative starting point for the construction of a transfer matrix, but at the expense of the introduction of complex weights.

We consider a loop model on a square $L \times M$ lattice $\mathscr{L}_M$ with periodic boundaries in the direction with system size L: the sites of the lattice are divided in M circular rows. There are free boundaries in the other direction, so that there are L 'dangling edges' which are connected to the vertices on row 1, and the same for row M. The partition function (see (1.2)) is

$$Z^{(M)} = \sum_{\mathscr{G}_M} u^{N_u} v^{N_v} w^{N_w} n^{N_l} \tag{2.1}$$

where M has been appended to indicate the number of rows. N_u, N_v and N_w are the number of vertices of $\mathscr{G}_M$ with weights u, v and w respectively, and N_l is the number of closed polygons on $\mathscr{G}_M$. In order to avoid confusion, we shall consistently refer to line segments connecting the vertices of $\mathscr{L}_M$ as 'edges', and to edges covered by $\mathscr{G}_M$ as 'bonds'. The allowed vertices are such that the bonds form polygons and chains. The latter may end only on the dangling edges of the vertices on row 1 or M (the presence of these dangling bonds corresponds with the presence of a magnetic field on the end rows in the spin representation of the O(n) model). Rows of vertical edges are numbered the same as the vertices immediately below them; thus, the rows of dangling edges are numbered 0 and M. The way in which some (or none) of the dangling edges of row M are covered by $\mathscr{G}_M$, and the way in which some (or none) of these dangling bonds are pairwise connected, is called 'connectivity' (see figure 2). Essential ingredients of the transfer matrix of the loop model are the evaluation of the number C_L of allowed connectivities on the L edges of row M (in particular for an invariant subset of these connectivities), and a mapping between these connectivities and the integers $1, 2, \ldots, C_L$. This bears some resemblance to the analogous problem in the cases of the Potts model [19, 20] and the cubic model [21]. The problem is worked out in the appendix for the loop model.

The natural numbers which label the allowed connectivities are denoted by Greek letters. Since the graph $\mathscr{G}_M$ determines the connectivity on the L dangling edges of row M, we can write this connectivity, β, as a function φ of $\mathscr{G}_M$:

$$\beta = \varphi(\mathscr{G}_M). \tag{2.2}$$

The partition function $Z^{(M)}$ is now divided into C_L restricted sums, $Z_\beta^{(M)}$, defined as follows:

$$Z_\beta^{(M)} = \sum_{\mathscr{G}_M} \delta_{\beta\varphi(\mathscr{G}_M)} u^{N_u} v^{N_v} w^{N_w} n^{N_l}. \tag{2.3}$$

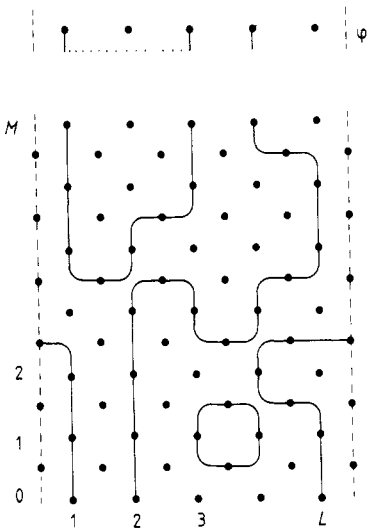

Figure 2. The graph $\mathcal{G}_M$ on an $L \times M$ lattice. The periodic boundaries in the L direction are indicated by broken lines. The connectivity $\varphi(\mathcal{G}_M)$ on row M is shown above: the points 1 and 3 are pairwise connected, point 4 is connected to one of the dangling bonds on row 1, and points 2 and 5 are unoccupied. The 'points' mentioned here are located in the middle of the vertical edges of row M, and are not to be confused with the vertices of the square lattice.

Thus $Z_\beta^{(M)}$ collects all terms in $Z^{(M)}$ which have connectivity β on row M, and

$$Z^{(M)} = \sum_\beta Z_\beta^{(M)}. \tag{2.4}$$

The next step is to consider the analogously restricted sum for a lattice $\mathcal{L}_{M+1}$ consisting of $M+1$ rows. The graph $\mathcal{G}_{M+1}$ is decomposed in the graph $\mathcal{G}_M$ on $\mathcal{L}_M$, and a graph g_{M+1} on row $M+1$, such that g_{M+1} fits the dangling edges covered by $\mathcal{G}_M$ on the M-row lattice. The total numbers of vertices with weights u, v and w are denoted N'_u, N'_v and N'_w respectively. Furthermore, we define N'_l as the number of closed loops on $\mathcal{G}_{M+1}$. Writing

$$N'_u = N_u + n_u \qquad N'_v = N_v + n_v \qquad N'_w = N_w + n_w \qquad N'_l = N_l + n_l \tag{2.5}$$

it is obvious that n_u, n_v, and n_w are the numbers of vertices of g_{M+1} of the types u, v and w respectively, and that n_l is the number of loops closed by appending g_{M+1} to $\mathcal{G}_M$. Thus

$$\begin{aligned} Z_\alpha^{(M+1)} &= \sum_{\mathcal{G}_{M+1}} \delta_{\alpha\varphi(\mathcal{G}_{M+1})} u^{N'_u} v^{N'_v} w^{N'_w} n^{N'_l} \\ &= \sum_{\mathcal{G}_M} u^{N_u} v^{N_v} w^{N_w} n^{N_l} \sum_{g_{M+1} \mid \mathcal{G}_M} \delta_{\alpha\varphi(\mathcal{G}_{M+1})} u^{n_u} v^{n_v} w^{n_w} n^{n_l} \end{aligned} \tag{2.6}$$

where the last sum is over those graphs g_{M+1} that fit $\mathcal{G}_M$. However, in order to determine which subgraphs g_{M+1} occur in this sum, not all information contained in $\mathcal{G}_M$ is required. It is enough to know which of the edges of row M are covered by $\mathcal{G}_M$, and this information is contained in $\varphi(\mathcal{G}_M)$. Likewise, in order to determine the second argument of the Kronecker delta, namely the connectivity $\varphi(\mathcal{G}_{M+1})$ on the dangling

edges, not all of $\mathcal{G}_{M+1}$ need be known. It is enough to know the connectivity $\varphi(\mathcal{G}_M)$ on row M and the subgraph g_{M+1}, as illustrated in figure 3. Thus

$$\varphi(\mathcal{G}_{M+1}) = \psi(\beta, g_{M+1}) \tag{2.7}$$

when $\beta = \varphi(\mathcal{G}_M)$. Substituting this in (2.6) gives

$$Z_\alpha^{(M+1)} = \sum_\beta \sum_{\mathcal{G}_M} \delta_{\beta\varphi(\mathcal{G}_M)} u^{N_u} v^{N_v} w^{N_w} n^{N_l} \sum_{g_{M+1}|\beta} \delta_{\alpha\psi(\beta, g_{M+1})} u^{n_u} v^{n_v} w^{n_w} n^{n_l}. \tag{2.8}$$

Since the third sum depends only on α and β (and not on other information contained in G_M) we can define the transfer matrix $\mathbf{T}$ by

$$T_{\alpha\beta} = \sum_{g_{M+1}|\beta} \delta_{\alpha\psi(\beta, g_{M+1})} u^{n_u} w^{n_w} v^{n_v} n^{n_l} \tag{2.9}$$

so that

$$Z_\alpha^{(M+1)} = \sum_\beta T_{\alpha\beta} Z_\beta^{(M)}. \tag{2.10}$$

Iteration of this equation gives, in vector notation

$$\boldsymbol{Z}^{(M+1)} = (\mathbf{T})^M \cdot \boldsymbol{Z}^{(1)}. \tag{2.11}$$

As in the case of the Potts model [20], memory and computer time requirements for a calculation involving the transfer matrix of a system with size L can be strongly reduced by the factorisation of $\mathbf{T}$ into L sparse matrices:

$$\mathbf{T} = \mathbf{T}_L \cdot \mathbf{T}_{L-1} \cdot \ldots \cdot \mathbf{T}_1 \tag{2.12}$$

where the $\mathbf{T}_i$ can be thought of as adding vertex i of a new row. A complication arises when the first vertex of a new row is added, because the number of dangling edges increases by two (see figure 4*a*, *b*). When more vertices are added, the number of dangling edges does not change, until $\mathbf{T}_L$ is applied and the number decreases by two. Thus, $\mathbf{T}_1$ is a $C_{L+2} \times C_L$ matrix, $\mathbf{T}_2, \ldots, \mathbf{T}_{L-1}$ are $C_{L+2} \times C_{L+2}$ matrices and $\mathbf{T}_L$ is a $C_L \times C_{L+2}$ matrix. The increase in the size of the matrices is outweighed by the fact that they are sparse—they contain only a few non-zero elements in each column. Their positions and values can be stored as one-dimensional arrays. A further memory reduction is possible because the $\mathbf{T}_i$ $(1 < i < L)$ are closely related. Let a permutation on the connectivities, obtained by cyclically renumbering the dangling edges $i \to i-1$, be expressed in the matrix $\mathbf{P}$. Then

$$\mathbf{T}_i = \mathbf{P}^{2-i} \cdot \mathbf{T}_2 \cdot \mathbf{P}^{i-2} \tag{2.13}$$

and

$$\mathbf{T} = \mathbf{T}_L \cdot \mathbf{P}^2 \cdot (\mathbf{P} \cdot \mathbf{T}_2)^{L-2} \cdot \mathbf{T}_1. \tag{2.14}$$

Thus, only three sparse matrices need be stored, namely $\mathbf{T}_L \cdot \mathbf{P}^2$, $\mathbf{P} \cdot \mathbf{T}_2$ and $\mathbf{T}_1$.

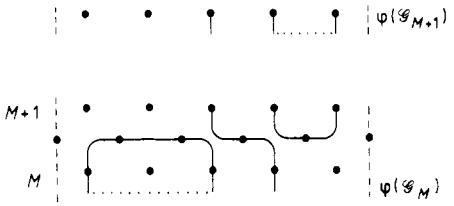

Figure 3. The connectivity $\varphi(\mathcal{G}_{M+1})$ on row $M+1$ (shown above) is determined by the graph g_{M+1} on row $M+1$ and the connectivity $\varphi(\mathcal{G}_M)$; other details of $\mathcal{G}_M$ are irrelevant. Furthermore, the change in the reduced energy due to the addition of g_{M+1} is also determined by $\varphi(\mathcal{G}_M)$ and g_{M+1}. In this example, $n_u = 2$, $n_v = 1$, $n_w = 2$ and $n_l = 1$ (see text).

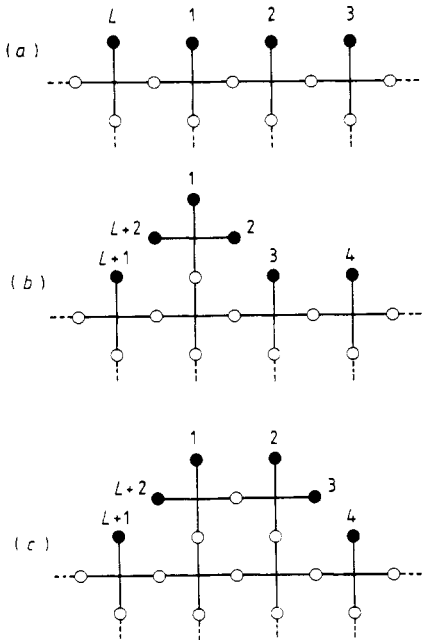

Figure 4. Topmost row of a finite O(n) model of width L. The circles shown are sites of the spins for the spin representation of the O(n) model. Bulk sites are shown as open circles, surface sites (i.e. dangling edges) as full circles. The transfer matrix $\mathbf{T}$, which adds a new row to the lattice, can be decomposed into L sparse matrices $\mathbf{T}_1, \mathbf{T}_2, \ldots, \mathbf{T}_L$, each of which adds one new vertex to the topmost row. (a) The situation after completion of a row. There are L dangling edges. (b) The situation after the addition of the first vertex of the new row, which is effectuated by $\mathbf{T}_1$. The number of dangling edges has now increased by two. (c) The situation after the addition of the second vertex of the new row, which corresponds with the action of $\mathbf{T}_2$. This operation leaves the number of dangling edges unchanged. The sparse matrices $\mathbf{T}_3, \ldots, \mathbf{T}_{L-1}$ are closely related to $\mathbf{T}_2$ (see text). Finally, the last sparse matrix $\mathbf{T}_L$ completes the next row so that we return to the situation shown in (a), with L dangling edges.

Expansion of $Z^{(1)}$ in (2.11) in eigenvectors of $\mathbf{T}$ shows that, in general, the free energy per vertex in the limit $M \to \infty$

$$f(L) = \lim_{M \to \infty} \frac{1}{LM} \log Z^{(M)} \tag{2.15}$$

is determined by the largest eigenvalue $\Lambda_L^{(0)}$ of $\mathbf{T}$ according to (1.9).

For actual computations it is useful to sort the connectivities by parity in 'odd' and 'even' sectors, according to the number n_d of bonds on the topmost row connected to the dangling bonds of row 0. Since this number can only decrease by multiples of 2 under the application of $\mathbf{T}$, the parity of the connectivities is conserved. Within the odd and even subspaces, one can introduce a further classification by ordering the connectivities according to the value of n_d. Since n_d can never increase, the transfer matrix $\mathbf{T}$ assumes an upper triangular shape in terms of the blocks generated by the groups of connectivities. Furthermore, on the basis of entropy considerations, we expect the largest eigenvalue of even sector to occur in the block with $n_d = 0$, and that of the odd sector in the block with $n_d = 1$.

At this point, it is useful to interpret this division of the loop model transfer matrix into blocks in terms of the O(n) spin model. If there is no field on row 0, the transfer matrix reduces to the $n_d = 0$ block. This shows that the free energy of the spin model with free boundaries is expressed by the leading eigenvalue of **T** (equation (1.9)) in the even sector, i.e. the $n_d = 0$ block. The diagram expansion of the O(n) model can also be used to transform spin-spin correlations into the loop-model language. Such correlations can be expressed in the weights of those loop diagrams in which the spins to be correlated are connected by $\mathcal{G}_M$. The information carried by the $n_d = 0$ connectivities includes the spin-spin correlations within a row. Energy-energy correlations between different rows (i.e. four-spin correlations) are also contained in the $n_d = 0$ block of **T**. On the other hand, the diagrams in the loop model which express the two-spin correlations between different rows are precisely those generated by the connectivities in the $n_d = 1$ block.

Details of the enumeration of the connectivities in the blocks of **T** with $n_d = 0$ and $n_d = 1$ are given in the appendix. In general, the invariant blocks of the transfer matrix are non-symmetric so that the usual methods to find the leading eigenvalues do not work. Thus we have applied the hybrid direct iteration-Hessenberg method described in [20].

By means of these techniques, we have numerically calculated the largest and second largest eigenvalues of **T** in the $n_d = 0$ block. Unless stated otherwise, we have restricted ourselves to translationally invariant eigenstates, i.e. the eigenvectors are invariant under multiplication by **P**. The range of the system size L was between 2 and 14. For the latter system size, the $n_d = 0$ block of **T** has a size of about $10^5 \times 10^5$ (see appendix). The leading eigenvalue in the $n_d = 1$ block was obtained for $L \leqslant 12$. These calculations were performed on the Convex-C1 minisupercomputer of Delft University.

3. Numerical results

Using the eigenvalues of the loop model transfer matrix, computed with methods explained in § 2 and the appendix for different system sizes, one can calculate the central charge and a few scaling dimensions as follows.

(1) The central charge. According to the theory of conformal invariance, the asymptotic finite-size scaling behaviour of the free energy $f(L)$ per site of an $L \times \infty$ system is given by (1.5), so that the central charge c can be estimated, using (1.9) and the eigenvalues $\Lambda_L^{(0)}$.

(2) The temperature exponent. The theory of conformal invariance predicts that the inverse correlation length has the asymptotic finite-size dependence given by (1.6). Thus, using the two leading eigenvalues of **T** in the $n_d = 0$ block, which determine the energy-energy correlation length according to (1.10), the temperature exponent X_T can be obtained.

(3) The magnetic exponent. Similarly, the magnetic exponent X_H corresponding to the spin-spin correlation function can be derived from the largest eigenvalue of **T** in the $n_d = 0$ sector and that in the $n_d = 1$ sector.

(4) Interface exponent 1. When the couplings, in this case in the corner-cubic interpretation, are antiferromagnetic, this will be manifested by an alternation of the leading eigenvalue as a function of L. The amplitude of the alternation can be interpreted as an 'interface energy'. This quantity can be analysed just as a correlation

length (in the Ising model, the interface energy and the inverse correlation length are related to each other by duality):

$$\xi_{\mathrm{int},1}^{-1}(L) = \tfrac{1}{2}\log(\Lambda_{L+1}^{(0)} + \Lambda_{L-1}^{(0)}) - \log \Lambda_L^{(0)} \qquad L \text{ odd.} \tag{3.1}$$

(5) Interface exponent 2. So far we have chosen $v \geqslant 0$. For even system sizes, the free energy does not depend on the sign of v. However, in general it does for odd L. Thus, a second interface exponent can be obtained on the basis of (3.1) using $v < 0$ for the odd system sizes, when the O(n) representation of the model is antiferromagnetic.

3.1. The extrapolation procedure

On the basis of (1.5) one can define finite-size estimates $f_\infty(1, N)$ and $c(1, N)$ of the bulk free energy and the central charge respectively by requiring

$$f(L) = f_\infty(1, N) + \frac{\pi c(1, N)}{6L^2} \tag{3.2}$$

for $L = N$ and $L = N+1$ (or $L = N$ and $L = N+2$ if $f(L)$ alternates as a function of L, in which case only even system sizes are used) so that both unknowns can be solved. For models at criticality, one may, in general, expect corrections to the leading finite-size dependence of the free energy proportional to larger negative powers of L. Therefore, $c(1, N)$ is expected to decay algebraically to c:

$$c(1, N) = c + aN^{-b} + \ldots . \tag{3.3}$$

Thus, a new series of estimates $c(2, N)$ can be obtained by solving

$$c(1, L) = c(2, N) + a(N)L^{-b(N)} \tag{3.4}$$

for $L = N$, $N+1$ and $N+2$ (if alternation as a function of L is absent). This new series of estimates is shorter, but it is expected to converge faster. They are called iterated fits. This process can be further iterated, yielding $c(3, N)$ etc. However, the series of estimates rapidly becomes too short to judge its apparent convergence, especially when $f(L)$ alternates as a function of L so that only the $f(L)$ data for even L are used as input for the fitting procedure. Moreover, numerical uncertainties in $f(L)$ due to rounding errors are strongly enhanced by this process of iteration, so that the best estimates were chosen as $c(2, N)$ or $c(3, N)$ for the largest available N.

Similar methods can be applied for the determination of the scaling dimensions. On the basis of (1.6) and (1.10) we define estimates $X_i(1, L)$ of X_i by

$$X_i(1, L) = \frac{L}{2\pi}\log\frac{\Lambda_L^{(0)}}{\Lambda_L^{(i)}}. \tag{3.5}$$

These estimates can be extrapolated by requiring

$$X_i(1, L) = X_i(2, N) + a(N)L^{-b(N)} \tag{3.6}$$

for $L = N$, $N+1$ and $N+2$ and solving for the unknowns. Alternatively, one may insert a fixed value $b(N) = 2$, so that two subsequent values of L suffice to find the iterated estimate $X_i(2, N)$. This is appropriate when Ising-like corrections to scaling dominate, but the results should converge also in other cases. Finally, the procedure can be further iterated, yielding $X_i(3, N)$. The process of iteration was ended on this point in most cases because of the reasons mentioned under the analysis of $f(L)$. Results of these fitting procedures are shown in the following subsections.

3.2. Numerical results for the central charge

Best estimates of the central charge, obtained by fitting procedures described in § 3.1, are given in table 1 for several values of n between -2 and $+2$ on each of the five branches defined in § 1. Estimated uncertainties in the last decimal places are shown between parentheses. Missing entries at $n=-2$ indicate that the finite-size data for the largest eigenvalue of **T** did not seem to correspond with the analytic continuation (as a function of n) of the rest of the branch. The data for branch 0, $n=-2$ and $n=-1.5$ do not correspond to the largest eigenvalue of **T**, but instead to the analytic continuation of the largest eigenvalue for $n>-1$; this level becomes the second largest eigenvalue for $n<-1$. In particular the results in table 1 on branches 1 and 2 are accurately determined, except for branch 1, $n=-2$ where the finite-size convergence is anomalously slow. They agree precisely with the central charge that was analytically derived for the critical and low-temperature branches of the O(n) model on the honeycomb lattice [6, 7], with the conjecture of Dotsenko and Fateev [12] and with that obtained by a mapping [13] of the O(n) model on the Gaussian model. Furthermore, the numerical results for branch 1 agree with those for the critical two-dimensional cubic model [13]. Thus, the conformal anomaly on branches 1 and 2 is accurately given by

$$c=1-6(g-1)^2/g \qquad \cos \pi g=-n/2 \qquad 0\leqslant g\leqslant 2 \tag{3.7}$$

where $g=2\theta/\pi$ (cf (1.4)) is the renormalised coupling constant.

Branch 1 corresponds with $g\geqslant 1$, branch 2 with $g<1$. The point at $n=-2$, branch 1 does not fit this expression very well. This is probably due to logarithmic corrections such as are present in the corresponding O(-2) model on the honeycomb lattice [6].

Table 1. Conformal anomaly of the square O(n) model for several values of n of the branches 0–4 as defined in § 1. These values were obtained by fitting a power law to the finite-size results for the free energy as described in the text. Estimated numerical uncertainties in the last decimal places are given between parentheses. In the case of branch 3, these inaccuracies are difficult to estimate (see text).

n	Branch 0	Branch 1	Branch 2	Branch 3	Branch 4
−2	−7.001 (4)	−1.88 (2)			
−1.5	−3.818 (2)	−1.0096 (1)	−14.4 (1)	−0.818 (3)	−14.3 (2)
−1	−2.00 (1)	−0.600 000 (1)	−7.000 (5)	−0.600 000 (1)	−6.52 (2)
−0.5	−0.820 (1)	−0.279 015 (5)	−3.8183 (3)	−0.34 (2)	−3.31 (1)
−0.25	−0.375 (1)	−0.135 732 (5)	−2.8011 (2)	−0.20 (1)	−2.299 (2)
0	0	0	−2.0000 (1)	0	−1.5000 (5)
0.25	0.318 (1)	0.130 070 (2)	−1.352 63 (5)	0.270 (5)	−0.853 (2)
0.5	0.588 (1)	0.255 950 (2)	−0.819 73 (2)	0.558 (1)	−0.320 (1)
1	1.003 (2)	0.500 000 (1)	0	1.003 (2)	0.500 000 (1)
1.5	1.27 (2)	0.741 840 (5)	0.587 57 (1)	1.270 (5)	1.088 (1)
2	1.40 (5)	1.000 00 (1)	1.000 01 (2)	1.5000 (2)	1.5000 (2)

These data show that branches 1 and 2 belong to the sets of O(n) universality classes as introduced by Nienhuis [3] for the honeycomb O(n) model.

The central charges on the other branches are less accurately determined numerically, but the data still strongly suggest two remarkable relations. In the first place,

the central charge of the O(n) model on branch 0 is, within numerical uncertainties of the order of 10^{-3}, equal to that of the O($n+1$) model on branch 2. We shall come back on this point in the discussion (§ 4). The entries at $n = 1.5$ and $n = 2$ for branch 0 in table 1 are exceptional in the sense that the fitting procedure did not clearly indicate finite-size convergence. Therefore, the numerical uncertainties shown between parentheses are rather uncertain themselves. In such cases, the number between parentheses is chosen to be, lacking a better criterion, to be ten times the difference between the last (i.e. those using the highest L values) two finite-size estimates. Under these circumstances, we consider the results for $n = 1.5$ and $n = 2$ on branch 0 consistent with non-algebraic finite-size dependence as expected in the absence of a second-order transition. Slow crossover phenomena, such as present in the q-state Potts model with q somewhat greater than four [19, 20], could mask the exponential finite-size convergence which is expected in the limit of large L.

Secondly, the estimates of the central charge for branch 4 suggest that the exact values are equal to those on branch 2 (for the same n) plus one half. This suggests the interpretation of branch 4 as a low-temperature O(n) phase with an additional Ising-like degree of freedom. This relation between branches 2 and 4 suggests that their continuations, i.e. branches 1 and 3 respectively, are similarly related. While this may be the case for $n \geqslant 1$, it is not so for $n \leqslant 0.5$. Our data indicate that slow crossover to a different type of behaviour occurs for $n < 1$. Convergence on that part of branch 3 appears to be good for $n = 0$ (no finite-size dependence of $f(L)$ for L even) and for $n = -1$ (this point appears to be closely related to the corresponding point of branch 1). For other values $n < 1$, the apparent convergence is poor. This implies not only that the error margins of the c values are relatively wide, but, as remarked above, also that the uncertainties themselves are difficult to assess.

3.3. The temperature exponent

Finite-size data for the energy-energy-like correlation length were used as input for the fitting procedure described in § 3.1. The results in terms of the temperature exponent X_T are shown in table 2.

The results for branch 0 can be identified with the exponent $2\Delta(m, m)$ as predicted by (1.7) and the Kac formula, equation (1.8). On this branch, level crossing occurs at $n = -1$, so that X_T changes sign. At $n = -1$, a second temperature dimension could be evaluated: $X_{T,2} = 0.750(1)$.

The data for branch 1, and branch 2 for $n \geqslant 1.5$, agree accurately with the temperature exponent X_T as conjectured by Cardy and Hamber [11], and derived by Nienhuis [3] for the honeycomb O(n) model. There is also good agreement with numerical results for the temperature exponent of that model [6] and of the n-component cubic model [21]. This exponent is identified as $2\Delta(1, 3)$ in the conformal block predicted by the Kac formula.

For branch 2, $n \leqslant 1$, the analytic continuation of the eigenvalues associated with X_T becomes dominated by other eigenvalues, at least for the range of finite-sizes that are accessible. Therefore, we have no X_T results on this branch for $n \leqslant 1$.

Again, the results for branch 3 exhibit strong crossover phenomena, so that we cannot rely on the convergence of the estimates, except for $n = 2$ and -1. The latter entry confirms the relation with the corresponding point on branch 1.

Finally, on branch 4 we find another confirmation of Ising-like degrees of freedom: $X_T = 1$, independent of n.

Table 2. Temperature critical dimension X_T of the O(n) model for several values of n on branches 0–4 as defined in § 1. These values were obtained from the finite-size results for the two largest eigenvalues in the $n_d = 0$ sector of the transfer matrix (see § 2). Estimated uncertainties in the last decimal places are given between parentheses. For a number of points on branches 0 and 3, these uncertainties were difficult to estimate (see text). Data are missing for most of branch 2 beacuse of level crossing: the second largest eigenvalue does no longer correspond to the critical dimension X_T.

n	Branch 0	Branch 1	Branch 2	Branch 3	Branch 4
−2	−0.5000 (3)	0.033 (3)			
−1.5	−0.191 70 (1)	0.2599 (3)		0.6101 (5)	1.000 (1)
−1	0	0.400 00 (1)		0.400 00 (1)	1.000 (1)
−0.5	0.138 570 (5)	0.530 98 (2)		0.2163 (2)	1.0001 (2)
−0.25	0.196 60 (1)	0.597 61 (3)		0.165 (5)	1.000 05 (5)
0	0.250 00 (1)	0.666 68 (3)		0.155 (5)	1.000 00 (1)
0.25	0.300 60 (1)	0.739 51 (3)		0.17 (1)	1.000 00 (1)
0.5	0.350 65 (2)	0.817 76 (1)		0.23 (1)	1.000 00 (1)
1.0	0.48 (1)	1.000 000 (1)		0.48 (1)	1.000 000 (1)
1.5	0.7 (2)	1.251 890 (1)	3.1951 (1)	1.1 (2)	1.000 000 (3)
2.0	0.9 (3)	2.000 000 (2)	2.000 000 (2)	1.0000 (2)	1.0000 (2)

3.4. The magnetic exponent

A similar procedure was followed for the magnetic correlation length. Results of the fitting procedure are shown in table 3. On branches 1 and 2, they agree with the prediction by Nienhuis [3] for the magnetic exponent of the honeycomb O(n) model, and with the exact results of Batchelor and Blöte [6]. This exponent is identified with the exponent $2\Delta((m+1)/2, (m+1)/2)$ in the theory of conformal invariance, where m parametrises the central charge according to (1.7). The results for branch 4 are, within numerical uncertainties, equal to the corresponding values on branch 2 plus the Ising value $X_H = 0.125$, again in agreement with the hypothesis that both Ising and O(n) degrees of freedom play a role in the physics of this branch. The entries for $n \leqslant 0$ on branch 4 in table 3 are based on eigenvalues which, for even L and $n_d = 1$,

Table 3. Magnetic critical dimension X_H of the O(n) model for several values of n on branches 0–4 as defined in § 1. These results were obtained from the ratio of the largest eigenvalues of the transfer matrix in the $n_d = 0$ and $n_d = 1$ sectors (see § 2). Estimated uncertainties in the last decimal places are given between parentheses.

n	Branch 0	Branch 1	Branch 2	Branch 3	Branch 4
−2	−0.500 (1)	0			
−1.5	−0.191 70 (5)	0.05375 (2)	−1.253 (5)	−0.17 (1)	−1.16 (1)
−1	0	0.0750 (2)	−0.6250 (5)	−0.12 (3)	−0.500 (5)
−0.5	0.138 57 (1)	0.090 96 (1)	−0.349 05 (5)	−0.10 (5)	−0.223 (1)
−0.25	0.196 60 (1)	0.097 843 (1)	−0.259 24 (1)	−0.08 (5)	−0.1342 (2)
0	0.2500 (1)	0.104 167 (2)	−0.187 500 (1)	−0.0 (1)	−0.062 50 (2)
0.25	0.3006 (1)	0.110 020 (1)	−0.128 569 (1)	0.1 (1)	−0.003 56 (1)
0.5	0.3505 (1)	0.115 442 (1)	−0.079 091 (1)	0.15 (5)	0.045 89 (1)
1.0	0.48 (1)	0.125 000 (1)	0	0.48 (1)	0.125 000 (1)
1.5	0.7 (1)	0.132 224 (1)	0.061 874 (1)	0.30 (2)	0.186 87 (1)
2.0	0.9 (3)	0.125 000 (1)	0.125 000 (1)	0.250 (1)	0.250 (1)

correspond with antisymmetric eigenvectors: they change sign under an elementary translation in the finite direction. For $n \geq 0.25$, the leading eigenvectors are symmetric. The difference is a consequence of the choice $v \geq 0$ in (1.4). Since w changes sign between $n = 0$ and $n = 0.25$, so does the $\pm$ sign in the definition of v.

A comparison with table 2 shows that the results for X_T and X_H are the same on branch 0. We explain this equality in § 4.

Again, the results on branch 3, and in particular their error margins, are poorly determined.

3.5. The interface exponents

We have also analysed the 'interface energy' which is interpreted here as the amplitude of the alternation of the free energy per row between even and odd values of L. This quantity can be analysed just as an inverse correlation length. Results of the fitting procedure are given in table 4 for branches 0, 3 and 4. Alternation is absent on branches 1 and 2. Note the discontinuity in the results for branch 4. This is a consequence of the choice $v \geq 0$ in (1.4), and the fact that for odd L, the largest eigenvalue depends on the sign of v (see also the remark in § 3.4). For $n > 0$, we observe the Ising magnetic exponent $\frac{1}{8}$.

Table 4. Critical dimension $X_{\text{int},1}$ corresponding with the vanishing of an 'interface' at a critical point. Such an interface may be created by e.g. antiperiodic boundary conditions or, as in the present case, if the O(n) spin-spin interactions are antiferromagnetic and the system size L is odd. Then, alternation as a fuction of system size occurs in the free energy, from which the interface exponent can be calculated (see text). Such alternation is absent on branches 1 and 2, and on branch 3 for $n \leq 0$. The discontinuity of the result on branch 4 is attributed to a change of sign of w between $n = 0$ and $n = 0.25$. Since v was chosen ≥ 0 in (1.4), branch 4 splits into two parts which are not each others analytic continuation. The part with $n \leq 0$ did not yield satisfactory finite-size convergence.

n	Branch 0	Branch 3	Branch 4
−2	−0.6250 (3)		
−1.5	−0.349 04 (1)	−0.0002 (5)	>1.5
−1	−0.1875 (1)	0.00000 (2)	>2
−0.5	−0.079 091 (1)	0.000 (1)	>2
−0.25	−0.036 781 (2)	0.000 (1)	>2
0	0	0	~2
0.25	0.032 512 (1)	0.004 (4)	0.125 00 (1)
0.5	0.061 87 (1)	0.02 (1)	0.125 000 (1)
1	0.121 (4)	0.121 (4)	0.125 000 (1)
1.5	0.18 (2)	0.126 (2)	0.125 000 (1)
2	0.28 (8)	0.125 000 (2)	0.125 000 (2)

A different exponent can be obtained by an analysis of the interface energy by choosing $v < 0$ in (1.4). These results are shown in table 5. For branches 1 and 2, they can be identified as the conformal exponent $2\Delta(1, 2)$. Note that, on branch 4, the Ising magnetic value now appears for $n \leq 0$. It is remarkable that the apparent convergence for branch 3 is quite reasonable, in contrast with other results presented above for

Table 5. Critical dimension $X_{\mathrm{int},2}$ corresponding with the vanishing of an interface at criticality for $v<0$ (see (1.4)). Such an interface can be due to antiferromagnetic interactions in the equivalent spin representation of the O(n) model if the system size L is odd. Then, alternation of the free energy per site as a function of L occurs, from which $X_{\mathrm{int},2}$ can be estimated. Such alternation can, in the loop model picture, be attributed to the fact that the energetically most favourable loop configurations discriminate between odd and even L. While a change of sign of v does not change the bulk free energy (nor the free energy for L even), it does influence the results for L odd and thereby the amplitude of the alternation. The entries for branch 4 with $n\leq 0$ are to be compared with those for $n>0$ in table 4: the underlying finite-size data are each others analytic continuation in n.

n	Branch 1	Branch 2	Branch 3	Branch 4
−2	−0.245 (5)			
−1.5	−0.152 50 (2)	10 (10)	−0.1525 (5)	0.10 (3)
−1	−0.100 03 (2)	3 (1)	−0.100 000 (1)	0.127 (5)
−0.5	−0.050 892 (1)	2.55 (5)	−0.0505 (10)	0.1250 (5)
−0.25	−0.025 906 (1)	2.27 (3)	−0.025 (1)	0.1250 (1)
0	0	1.999 (2)	0	0.125 00 (5)
0.25	0.027 322 (1)	1.778 (1)	0.032 (2)	1.90 (1)
0.5	0.056 659 (1)	1.5842 (5)	0.0667 (1)	1.710 (5)
1	0.125 000 (1)	1.2500 (1)	0.121 (4)	1.375 (1)
1.5	0.219 459 (1)	0.948 19 (5)	0.24 (1)	1.0732 (1)
2	0.500 001 (2)	0.500 001 (2)	0.630 (5)	0.630 (5)

branch 3. There is a striking similarity with branch 1 in this table, at least for $n\leq 0$. Table 5 does not contain data for branch 0, because $v=0$ in this case.

4. Discussion

There are two major clues to the universality class of the critical points we have analysed. The first is value of the conformal anomaly c, which gives clear evidence that the five critical points for each value of n, are generally in distinct classes. Most of the critical behaviour we find can be related to that of the unitary series [9] of which the central charge and the values of the critical exponents are given by (1.8). The second clue is the location in the space of coupling constants u, v and w, which in some cases gives an indication of the type of critical behavior to be expected there. In the following discussion we will use the points at $n=0$ as the guiding example because they are in the middle of the branches $-2<n<2$. Also the case $n=1$ will be used for guidance especially where exact results are available.

4.1. Branches 1 and 2

On branch 1, as indicated in the previous section, the results for the conformal anomaly and the critical exponents are in excellent agreement with those of the ordinary O(n) critical points. Figure 5 shows the numerical values of c plotted against n, together with the analytically known results (equation (3.7)), with $1<g<2$ and $m=1/(g-1)$. The agreement is found over the full range of n, also in the exponents X_T, X_H and $X_{\mathrm{int},2}$, which are identified as $2\Delta(1,3)$, $2\Delta((m+1)/2,(m+1)/2)$ and $2\Delta(1,2)$ respectively.

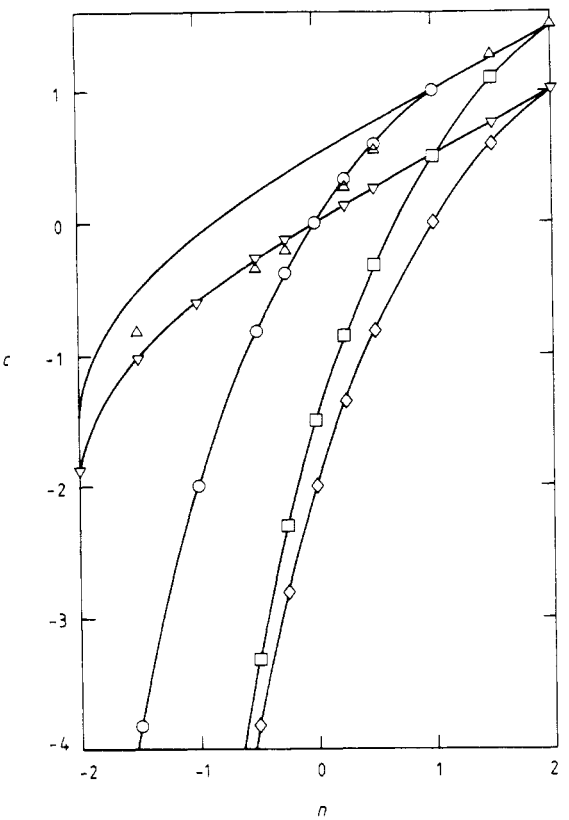

Figure 5. Conformal anomaly for the five branches of the O(n) model defined in § 1. The data points, namely ○: branch 0; ▽: branch 1; ◇: branch 2; △: branch 3; □: branch 4, are the results of our numerical analysis described in § 3. The full curves are the known analytic results for branches 1 and 2 of the honeycomb O(n) model, the same results, but displaced by +0.5 in the c direction and the result for branch 2, displaced by −1 in the n direction. The identification of the numerical results is quite clear except in the case of branch 3, where finite-size convergence was rather poor.

For $n = 0$ the model describes the scaling limit of long polymers in dilute solution. The critical point can be viewed as the transition where the chemical potential of the monomers balances with the configurational entropy. When the excluded volume interaction is ignored this transition would take place at $2u + v = 1$, which is indeed not far from the $n = 0$ critical point on branch 1: $(u, v, w) = (0.4, 0.3, 0.1)$ from (1.4). Furthermore since $w < u^2$, there is no attractive force between spatially adjacent monomers, and we conclude that this point describes the ordinary self-avoiding walk (SAW). In the Ising case $n = 1$, the critical point on branch 1 turns out to satisfy the free fermion condition $2w = 2u^2 - v^2$, and is therefore exactly soluble [22 and references therein], both at criticality and away from it.

As in the honeycomb O(n) model, the critical point on branch 1 can be analytically continued through $n = 2$ into branch 2, which is considered, from the large values of the coupling constants, to govern the low-temperature behaviour of the model. Also on this second branch, our results for the magnetic exponent are in excellent agreement with the analytical predictions from $2\Delta((m+1)/2, (m+1)/2)$ of (1.8) and (3.7), now with $0 < g < 1$ and $m = g/(1-g)$. The thermal exponent was determined for $n \geq 1.5$

only because of its large value, which makes it susceptible to masking by other eigenvalues.

4.2. Branches 3 and 4

On branch 4 we observed that the data for the central charge are accurately given by those on branch 2, increased by $\frac{1}{2}$. This suggests that the model can be described as a superposition of an Ising model and an O(n) model. There appears to be a similar situation in the SOS model which was investigated recently by den Nijs and Rommelse [23, 24]. When the coupling between the two simultaneously critical systems is irrelevant, the central charge is simply the sum of those of the component models. A similar behavior is seen in frustrated XY models [25, 26 and references therein], for the description of arrays of Josephson junctions [27], which have a central charge $\frac{3}{2}$. In fact, the limit $n = 2$ of branch 4 may well be the description of precisely that system. The thermal exponent has the Ising value 1 over the full range of n, while the magnetic exponent turns out to be the sum of the O(n) exponent of branch 2 and the Ising value $\frac{1}{8}$.

The role of the class of critical points of branch 4 in the phase diagram is not so obvious as for the first two branches. We observe that the Ising case again satisfies the free fermion condition and corresponds, in the corner-cubic representation, to an antiferromagnetic critical point. In the language of the loop gas this is a transition between a random packing of polygons and a dense packing. Thus for polymers it is a transition between a dense solution and a melt. Since a dense packing of polygons is lattice dependent, the same may be expected of the nature and existence of this transition.

The value of the central charge on branch 3 could not be determined as accurately as on the other branches. It is, however, clear that the analytic continuation of the value on branch 4 does not fit the data, except possibly for $n \geqslant 1$. The location of these points in the phase diagram (e.g. at $n = 0$, $(u, v, w) = (0.4, 0.1, 0.5)$) suggests that they may be tricritical points. This can be seen by the following reasoning. In an intersection of the phase diagram with $u = v$ (figure 6), an ordinary critical point is expected on the u axis. On the w axis there must be a first-order transition between a completely empty lattice and one fully packed with polygons. Somewhere in between these two extremes the simplest scenario requires a tricritical point where the transition changes form second to first order. Therefore, in the limit $n = 0$, we have here a candidate for the theta transition of polymer solutions. For the Ising case $n = 1$ (see below) the point on branch 3 is tetracritical and has two critical lines emerging from it. This scenario, indicated by the broken curve in figure 6, may also be valid for $n = 0$. In this respect it should be noted that the thermal exponent $X_T = 0.15$, even with the fairly large error bar of 0.01, seems to disagree with the value $\frac{1}{4}$ proposed by Duplantier and Saleur [28].

A different interpretation is suggested by the numerical evidence noted in § 3.5 for a relation between branches 1 and 3 for $n \leqslant 0$, which indicates that the point $n = 0$ on branch 3 may be an ordinary SAW point. Such a relationship is in line with a link between branches 2 and 4 (i.e. the analytic continuations of branches 1 and 3) noted above. Our results may indicate that, for n smaller than some special value, crossover takes place to ordinary critical O(n) behaviour. If this is true, the question remains why the relation between branches 1 and 3 does not show up in the analysis of the central charge, and for the other exponents. We have at present no good explanation

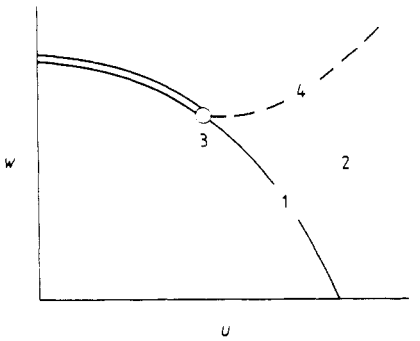

Figure 6. The role of the critical points of branches 1-4 in the qualitative phase diagram, shown here as an intersection through the w axis, e.g. the plane $u = v$ or $v = 0$ for $n = 0$. Unless $u = 0$, the precise ratio of u and v is not expected to affect the qualitative picture. A first-order transition cuts the w axis, and a continuous transition takes place on the horizontal axis. Supposedly these two points are connected by a transition line which changes from first to second order in a multicritical point (3). Another continuous transition line (4) may emerge from this point. The numbers of this figure show a qualitative location of the branches 1-4.

why slowly converging crossover effects should (approximately) cancel only in the analysis of the exponent $X_{\text{int},2}$. Especially at $n = -1$, the numerical evidence relating branches 1 and 3 is strong. For small system sizes, we have evaluated the whole eigenspectrum and observed that most, but not all, of the eigenvalues match precisely. Comparison of the vertex weights shows that u and v are identical, but that w is different for branches 1 and 3 (for $n = -1$). In order to understand the exact equivalence of the two O(−1) models, consider a loop model configuration in the $n_d = 0$ sector, in which two loop segments collide in a vertex of type w. A configuration with opposite weight is obtained by rotating the w-type vertex, because the number of loops changes by one. Since the sum of the contributions to the partition function cancels, vertices of type w are, in effect, forbidden. This equivalence applies also to the $n = -1$ points on branches 2 and 4. The paradox that the central charges are nevertheless different is due to the fact that they were, in all cases, determined from the largest eigenvalue of T. However, the corresponding eigenvector may be such that its contribution to the partition function of a system without dangling bonds vanishes.

At $n = 1$ the critical point of the third branch simplifies by the fact that v vanishes and that the two vertex configurations with weight w need not be distinguished. Thus only six vertices remain which can be mapped onto F-model configurations by the following procedure. One divides the sites of the lattice into two interpenetrating sublattices A and B. The diagrams of the model are transformed by replacing occupied horizontal and empty vertical edges by arrows from A to B and occupied vertical and empty horizontal edges by arrows from B to A. Thus the model is turned into an F model precisely at its transition point. In the phase diagram this point does not play the role of a tricritical, but of a tetracritical point, where the Ising ferro- and antiferromagnetic transitions merge into a single first-order transition [29, 30]. It is not obvious whether this qualitative behaviour persists at other values of n. It should be noted that at $n = 1$ in any case this behaviour is not that of an isolated point, but that the entire Baxter line [31], ($2u + v = 1$, $w = \frac{1}{2}$) is tetracritical. The central charge and critical exponents are not the known tricritical values ($c = \frac{7}{10}$, $X_T = \frac{1}{5}$ and $X_H = \frac{3}{80}$), but $c = 1$, $X_T = \frac{1}{2}$ and $X_H = \frac{1}{8}$, as corroborated by the numerical results.

When speculating about the possible generalisation of the qualitative shape of the Ising phase diagram to other values of n, it should be noted that at $n = 1$ the branches 0 and 3 intersect, indicative of a crossover between two types of behaviour. Another complication is the existence of two marginal operators, namely those that span the Baxter line and the F model respectively. This may have a negative effect on the numerics both at this point and in the neighbourhood, and explain the relative inaccuracy of our results.

4.3. Branch 0

In the separate branch 0 we find again a new set of universality classes. In § 3, we observed that the central charge of this family of critical points is equal to that in branch 2, apart from a displacement of n. In retrospect we could understand this fact as follows. In the limit $u = v = 0$ and $w = \infty$, all edges are occupied in the surviving diagram configurations. The partition sum, however, is non-trivial, because each vertex still carries a degree of freedom in the two ways that the four bonds can be connected. This affects the weight of each configuration through the number of polygons by which the lattice is covered. The system has been recognised [32] as the n^2-state Potts model at its critical point. Here it is more appropriate to view it as an O(n) model in its low temperature phase, that is in the same universality class as branch 2. The equivalence between these two models has been noted before [3, 28]. The partition sum, up to a constant power of w, is simply the sum of n^p over all covering polygon configurations, with p the number of polygons. This is rewritten by setting $n = n' + 1$, and summing over all coloured polygon configurations, in which each polygon is either red with weight n', or blue with weight 1. Summation over the colouring alone trivially recovers the original partition sum. Another useful partial summation is over all possible blue polygon configurations given the red ones. Since the weight of the blue polygons is trivial, this sum can be performed yielding new effective weights to the configurations in figure 1, now of the remaining red polygons only. Thus each vertex which is clear of all red polygons has weight two, since there are two ways in which this vertex can be covered by blue polygons. Vertices touching on one or two red polygons allow only one blue configuration, and thus have weight one. Therefore, relative to the empty vertex the new weights are

$$u' = \tfrac{1}{2} \qquad v' = 0 \qquad w' = \tfrac{1}{2} \qquad n' = n - 1 \tag{4.1}$$

—precisely those of branch 0. This explains why the central charges of branch 0 and 2 are related via a shift in n by one. It may be noted that this relation is generalisation of that found by Duplantier and Saleur [28] between the supposed theta point of polymers ($n = 0$) and the low-temperature Ising ($n = 1$) model. The equivalence between the branches 0 and 2 can also be used to predict the value of various exponents. Indeed the thermal exponent on branch 0 can be explained as the polarisation exponent of the O(n) model on branch 2 [4] since the correlation function of the polarisation operator is the probability that two vertices are connected by a single polygon. This exponent has been identified [28] with $(p, q) = (m, m)$ in the conformal grid, in good agreement with the numerical data in the range $-2 < n < 1$, where the equivalence is valid. The magnetic exponent governs the correlation function between the two ends of an open chain. One would be tempted to identify this with the exponent $2\Delta((m+1)/2, (m+1)/2)$, the magnetic exponent of the equivalent O($n+1$) model. However, in the associated covering polygon configurations the terminals of an open chain cannot

be embedded. The way to map the open chain on an allowed set of configurations in the polygon covering model is to identify the endpoints of the chain as points where a red polygon changes into a blue one. Obviously the correlation function between two such operators is equal to the probability that the two operators sit on the same polygon. But this correlation function we just identified as the thermal one. Thus we expect equality between the thermal and magnetic exponents on branch 0, as corroborated by the numerical data. In contrast, the values $2\Delta[(m+1)/2, (m+1)/2]$ appears as the interface exponent (table 4).

Since we used the location of the critical points in the *uvw* space as a qualitative cue to their physical meaning, we are now confronted by the problem that the points on branch 0 and 3 are relatively close. Therefore both points are candidates for the same role in the phase diagram. Within the $v = 0$ plane, again using $n = 0$ as a guide for other values of n, we expect a critical (in this case SAW) point, as well as a tricritical point, with a phase diagram like figure 6. This indicates the point on branch 0 as the tricritical point within this subspace, indeed the same role as we gave to branch 3. Since the two points do not appear to be in the same universality class, from their value of c, and even more so from the value of the thermal exponent, we now have two candidates for the tricritical point. However, we shall show that branch 0 is threefold unstable in the space of u, v and w, and thus cannot be an ordinary tricritical point, though it may play this role in the special symmetry plane $v = 0$.

Within the *uw* plane we find two correlation functions with relevant exponents. There is in the first place the thermal exponent governing the probability that two distant points sit on the same polygon and are thus connected by two lines. This operator is the thermodynamic conjugate of u. To get the exponent associated with w, one should inspect the probability function that two points are connected by four lines. This also follows readily from the Coulomb gas approach and turns out to be the conformal exponent $2\Delta(m, m-1)$. This next-to-leading exponent turns out to be also relevant in the entire range $-2 < n < 1$, and is marginal at $n = 1$, as expected from the equivalence with the F model. Since we computed only leading exponents in each sector we have no numerical data for this exponent, except at $n = -1$, where the leading thermal exponent happened to vanish (see § 3.3). At this point the numerical value agrees accurately with the analytical value of $\frac{3}{4}$.

The exponent associated with v governs the correlation function between two straight segments in a polygon configuration which meanders everywhere else. In order to map these configurations onto covering polygon configurations we again use the rule that bonds are turned into red lines and empty edges into blue lines. Thus the diagrams of the correlation function between the two straight segments are mapped into configurations of red and blue polygons two of which intersect, leaving the crossing points connected by four lines. For this reason the exponent associated with the weight v is equal to that of w, and we have a total of three relevant exponents in the thermal sector of the model. Therefore the points of branch 0 only govern critical behaviour in the $v = 0$ plane. In this subspace they play the same role as branch 3 in the rest of the *uvw* space, but they are probably of a different universality class.

4.4. Special cases

While most of the discussion applies to entire branches, there are some specific points which deserve special attention. As mentioned above, there is in the first place the intersection at $n = 1$ of branch 0 and branch 3, where the model reduces to the transition

point of the F model. The point $n = 1$ on branch 2 is equivalent to a trivially solvable, disordered Ising model with four-spin interactions on the elementary faces. The $n = 1$ points of branches 1 and 4 map onto critical free-fermion models with ferromagnetic and antiferromagnetic nearest-neighbour interactions respectively. Besides, we note again the equivalence between the points $n = -1$ of the branches 1 and 2 with those of branches 3 and 4 respectively.

Besides the O(n), corner-cubic and loop gas representation of the partition sum, we can also write it as a 19-vertex model. This connection is made, just as in the case of the honeycomb model [3], by placing arrows on the bonds, thus giving a fixed but arbitrary orientation to each loop. It turns out that at the points $n = 2$ of our branches 1 and 2 (or 3 and 4) the model is equivalent to the 19-vertex model of Zamolodchikov and Fateev (ZF) [33]† at the point $\gamma = 3\pi i/4$ ($\pi i/4$). A major consequence of this equivalence is that the central charge, which assumes the two different values 1 and $\frac{3}{2}$ at these two points, cannot be a constant in the whole of the ZF model. Alcaraz and Martins [34] recently found $c = \frac{3}{2}$ in the regime $0 \leqslant -i\gamma \leqslant \pi/2$, generalising an earlier result of Affleck [35] for $\gamma = 0$.

The 19-vertex representation opens the way to yet another formulation of the model. The arrows can be interpreted as spin states of a spin-1 particle. Then the transfer matrix can be written in terms of angular momentum operators. In general this form is fairly complicated and unenlightening, but in one case, that is when $n = 2$ on branch 0, it reduces to the (ordered) product

$$\mathsf{T} = \prod_{j=1}^{L} \tfrac{1}{2}(\boldsymbol{S}_j \cdot \boldsymbol{S}_{j+1})^2 \tag{4.2}$$

where the $\boldsymbol{S}$ are spin-1 angular momentum operators. The isotropy of this formulation, i.e. the O(3) symmetry, is a manifestation of the above-mentioned equivalence of branch 0 to an O(n+1) model. This model is not critical but it is solvable as we know from its equivalence to the nine-state Potts model at its first-order transition point [36, 37]. It implies that we have here another solvable isotropic spin-1 quantum chain.

Acknowledgment

This work was supported in part by the KNAW (Royal Netherlands Academy of Sciences).

Appendix. Enumeration of the connectivities

The process of constructing the partition function of an O(n) model on an $L \times M$ lattice by means of the loop model transfer matrix was described in § 2. For actual calculations, we require an enumeration of the L-point connectivities, that is the ways in which the L points on the dangling edges of row M are connected by the graph $\mathcal{G}_M$. Each of the L points has three possibilities:

(1) the point can be vacant, that is not covered by $\mathcal{G}_M$;

(2) the point can be connected by $\mathcal{G}_M$ to one of the dangling bonds of row 0;

(3) the point can be connected by $\mathcal{G}_M$ to one and only one other point on row M.

† Equation 2.5f of that paper contains an error; the correct expression follows from its equation (A.16).

These possibilities are determined by the graph expansion of the O(n) model in the absence of a bulk magnetic field. There exists a restriction to the ways in which the points on row M can be pairwise connected by $\mathcal{G}_M$. If $i<j<k<l$, and points i and k are connected, then points j and l cannot be connected, because loops are not allowed to intersect. Here we consider only the 'allowed' connectivities which satisfy this restriction. Moreover, we restrict ourselves to two subsets of the connectivities, namely the connectivities without points connected to the dangling bonds of row 0 (the $n_d=0$ connectivities), and the connectivities with one and only one point connected to row 0 (the $n_d=1$ connectivities). These two subsets require different enumerations. The $n_d=0$ connectivities serve to derive the free energy and the energy-like correlation length, while the $n_d=1$ connectivities serve to derive the magnetic correlation length. For this reason, we refer to the $n_d=0$ connectivities as non-magnetic, and to those with $n_d=1$ as magnetic ones. The problem of the enumeration of these connectivities will be solved in three steps: (1) the enumeration of the 'dense connectivities': a subset of the non-magnetic connectivities, namely the $n_d=0$ connectivities without vacant points, (2) the enumeration of the non-magnetic connectivities and (3) the enumeration of the magnetic connectivities.

(1) The enumeration of the dense connectivities on 2m points appears to be closely related to that of the 'restricted connectivities' in the case of the Potts model [19, 20]. For clarity, we use a notation that is similar to that used in [20]. Consider a row of 2m points, all of which are pairwise connected. This connectivity can be represented by a row of 2m positive integers $(i_1, i_2, \ldots, i_{2m})$ such that $i_k=i_l$ if points k and l are connected, and $i_k\neq i_l$ otherwise. The condition that loops are well nested (i.e. they do not intersect) excludes the situation $j<k<l<n$, $i_j=i_l$ and $i_k=i_n$. The number of distinct, dense connectivities on 2m points is denoted c_m. A recursion relation for c_m follows immediately from the well nestedness condition. Point 1 must be connected to one and only one other point; and the position of that point has to be even. Thus there exists a number k such that $i_1=i_{2k}$. Since $i_j\neq i_l$ for $1<j<2k$ and $2k<l\leqslant 2m$, the connectivity decomposes into two independent pieces when points 1 and $2k$ are removed: one piece consists of $2k-2$ points, and the other of $2m-2k$ points. Therefore

$$c_m=\sum_{k=1}^{m} c_{k-1}c_{m-k} \tag{A1}$$

with $c_0=1$.

Next, define a generating function $P(x)$ as

$$P(x)=\sum_{m=0}^{\infty} c_m x. \tag{A2}$$

Substitution of the recursion (A1) gives

$$P(x)=1+\sum_{m=1}^{\infty}\sum_{k=1}^{m} c_{k-1}c_{m-k}x^m=1+x\sum_{k=1}^{\infty}\sum_{m=k}^{\infty} c_{m-k}x^{m-k}c_{k-1}x^{k-1}=1+xP^2(x). \tag{A3}$$

The correct solution of this equation is

$$P(x)=(1-\sqrt{1-4x})/(2x). \tag{A4}$$

Taylor expansion of $P(x)$ shows that

$$c_m=\{(4n-2)/(n+1)\}c_{m-1} \tag{A5}$$

which implies, since $c_0=1$,

$$c_m=(2m)!/\{m!(m+1)!\}. \tag{A6}$$

This is the same expression as for the number of m-point connectivities in the case of the Potts model. In the limit $m \to \infty$ we observe that $c_m \sim 4^m$.

In order to establish a correspondence between the dense connectivities on 2m points and the integers $1, 2, \ldots, c_m$ we represent connectivities by a row of positive integers as mentioned above. A function ρ is defined on these rows as

$$\rho(i_1, i_2, \ldots, i_{2m}) = k \tag{A7}$$

where k is determined by $i_1 = i_{2k}$. The function ρ enables one to define an ordering of the 2m-point dense connectivities by the following recursive rule. The connectivity $(i_1, i_2, \ldots, i_{2m})$ precedes the connectivity $(j_1, j_2, \ldots, j_{2m})$ if one of the three following conditions is satisfied:

(i) $\rho(i_1, i_2, \ldots, i_{2m}) < \rho(j_1, j_2, \ldots, j_{2m})$;

(ii) $\rho(i_1, i_2, \ldots, i_{2m}) = \rho(j_1, j_2, \ldots, j_{2m})$ and $(i_{2k+1}, \ldots, i_{2m})$ precedes $(j_{2k+1}, \ldots, j_{2m})$;

(iii) $\rho(i_1, i_2, \ldots, i_{2m}) = \rho(j_1, j_2, \ldots, j_{2m})$ and $(i_{2k+1}, \ldots, i_{2m}) = (j_{2k+1}, \ldots, j_{2m})$ and $(i_2, \ldots, i_{2k-1})$ precedes $(j_2, \ldots, j_{2k-1})$

where k is determined by (A7). The meaning of the second equality of (iii) is that $i_l = i_n$ if and only if $j_l = j_n$. If these conditions do not provide a decision which connectivity precedes the other, the connectivities are equal. On the basis of these conditions, the unique number $\sigma(i_1, i_2, \ldots, i_{2m})$ of a $2m$-point connectivity is determined recursively as follows:

$$\begin{aligned} &\sigma(i_1, i_2, \ldots, i_{2m}) = 1 \qquad \text{if } m = 0 \text{ or } m = 1 \\ &\sigma(i_1, i_2, \ldots, i_{2m}) = \sum_{l=1}^{k-1} c_{l-1} c_{m-l} + c_{k-1}\{\sigma(i_{2k+1}, \ldots, i_{2m}) - 1\} + \sigma(i_2, \ldots, i_{2k-1}) \end{aligned} \tag{A8}$$

where k is determined by (A7). The first term on the right-hand side is the number of connectivities $(j_1, j_2, \ldots, j_{2m})$ for which $\rho(j_1, j_2, \ldots, j_{2m}) < k$. The second term is the number of connectivities with $\rho(j_1, j_2, \ldots, j_m) = k$ and for which $\sigma(j_{2k+1}, \ldots, j_{2m}) < \sigma(i_{2k+1}, \ldots, i_{2m})$. Finally, the third term is the number of $(2k-2)$-point connectivities which precede $(i_2, \ldots, i_{2k-1})$, plus one.

(2) The enumeration of the non-magnetic connectivities. At present, we consider connectivities which have, apart from a number of pairwise-connected points, also a number of points that are 'vacant', i.e. not connected to any other point. The enumeration of these connectivities resembles that of the 'general connectivities' in the case of the Potts model in a magnetic field [19] or with vacancies. The L-point non-magnetic connectivities of the loop model are now represented by a row of non-negative integers $(i_1, i_2, \ldots, i_L)$ such that

$$\begin{cases} i_k = 0 & \text{if and only if point } i \text{ is vacant} \\ i_l = i_m > 0 & \text{if and only if point } l \text{ is connected to point } m. \end{cases}$$

Consider such a connectivity with precisely p pairs of connected points ($0 \leqslant p \leqslant [L/2]$, where $[L/2]$ stands for the integer part of $L/2$). There are also $L - 2p$ vacant points, which can be distributed in $\binom{L}{2p}$ ways. The connectivities on the $2p$ points that are not vacant are precisely the dense connectivities described earlier. Thus, the total number a_L of non-magnetic connectivities on L points is

$$a_L = \sum_{p=0}^{[L/2]} \binom{L}{2p} c_p = \sum_{p=0}^{[L/2]} \frac{L!}{p!(p+1)!(L-2p)!}. \tag{A9}$$

An ordering of these connectivities can be obtained from the number of zeros, a lexicographic ordering on the basis of the zeros, and the dense connectivity that remains when the zeros are removed. For the lexicographic part of the enumeration, we recursively define a function ψ on a row of m non-negative integers with w non-zeros:

$$\psi(i_1, i_2, \ldots, i_m) = \begin{cases} 1 & \text{if } w = 0 \text{ or } m = 1; \\ \psi(i_2, \ldots, i_m) & \text{if } i_1 \neq 0; \\ \binom{m-1}{w} + \psi(i_2, \ldots, i_m) & \text{if } i_1 = 0. \end{cases}$$

Consider a connectivity $(i_1, i_2, \ldots, i_L)$ with u connected pairs. Denote by $(j_1, j_2, \ldots, j_{2u})$ the sequence that remains when the zeros are removed. A unique number τ is assigned as follows:

$$\tau(i_1, i_2, \ldots, i_L) = \sum_{k=u+1}^{[L/2]} \binom{L}{2k} C_k + \{\psi(i_1, i_2, \ldots, i_L) - 1\} C_u + \sigma(j_1, j_2, \ldots, j_{2u}). \quad \text{(A10)}$$

The first term on the right-hand side is the number of connectivities with more than u pairs of non-zeros. The second term is the number of connectivities with u pairs of non-zeros that precede $(i_1, i_2, \ldots, i_L)$ on the basis of the lexicographic ordering. Finally, the last term is the number of connectivities that precede $(i_1, i_2, \ldots, i_L)$ on the basis of the ordering of the dense connectivities that remain when the zeros are removed, plus one.

(3) The enumeration of the magnetic connectivities. In addition to connected pairs and vacant points, we now also have one point (with position k) connected to a dangling bond of row 0. We associate this point with an integer $i_k = -1$ in the row $(i_1, i_2, \ldots, i_L)$ that represents the magnetic connectivity. Since there is no restriction on k, the total number b_L of magnetic connectivities is

$$b_L = L a_{L-1}. \quad \text{(A11)}$$

Table 6. The total number a_L of $n_d = 0$ connectivities and the number b_L of $n_d = 1$ connectivities are given for several values of L. Calculations in the $n_d = 0$ (non-magnetic) subspace were performed up to finite size 14, which necessitated the enumeration of the connectivities up to $L = 16$. Calculations for the $n_d = 1$ (magnetic) subspace were performed up to systems of size 12, so that magnetic connectivities up to $L = 14$ had to be enumerated.

L	a_L	b_L
2	2	2
3	4	6
4	9	16
5	21	45
6	51	126
7	127	357
8	323	1 016
9	835	2 907
10	2 188	8 350
11	5 798	24 068
12	15 511	69 576
13	41 835	201 643
14	113 634	585 690
15	310 572	
16	853 467	

These connectivities are ordered on the basis of the value of k and the ordering of the non-magnetic connectivities. Thus, the number ω associated with the connectivity is

$$\omega(i_1, i_2, \ldots, i_L)=(k-1)a_{L-1}+\tau(i_1, i_2, \ldots, i_{k-1}, i_{k+1}, \ldots, i_L).$$

The numbers a_L and b_L are given in table 6 for several values of L. For large L, the leading power-law behaviour of a_L and b_L is given by

$$\lim_{L\to\infty} \frac{a_L}{a_{L-1}}=\lim_{L\to\infty} \frac{b_L}{b_{L-1}}=3. \tag{A12}$$

Inverse algorithms, which map positive integers onto the connectivities, can be constructed by similar methods.

References

[1] Stanley H E 1974 *Phase Transitions and Critical Phenomena* vol 3, ed C Domb and M S Green (London: Academic)
[2] Domany E, Mukamel D, Nienhuis B and Schwimmer A 1981 *Nucl. Phys.* B **190** [FS3] 279
[3] Nienhuis B 1982 *Phys. Rev. Lett.* **49** 1062
[4] Nienhuis B 1987 *Phase Transitions and Critical Phenomena* vol 11, ed C Domb and J L Lebowitz (London: Academic)
[5] Baxter R J 1986 *J. Phys. A: Math. Gen.* **19** 2821; 1987 *J. Phys. A: Math. Gen.* **20** 5241
[6] Batchelor M T and Blöte H W J 1988 *Phys. Rev. Lett.* **61** 138; 1989 *Phys. Rev.* B **39** 2391
[7] Suzuki J 1988 *J. Phys. Soc. Japan* **57** 2966
[8] Belavin A A, Polyakov A M and Zamolodchikov A B 1984 *J. Stat. Phys.* **34** 763
[9] Friedan D, Qiu Z and Shenker S 1984 *Phys. Rev. Lett.* **52** 1575
[10] Cardy J L 1987 *Phase Transitions and Critical Phenomena* vol 11, ed C Domb and J L Lebowitz (London: Academic)
[11] Cardy J L and Hamber H W 1980 *Phys. Rev. Lett.* **45** 499
[12] Dotsenko V S and Fateev V A 1984 *Nucl. Phys.* B **240** 312; 1985 *Nucl. Phys.* B **251** 691
[13] Blöte H W J, Cardy J L and Nightingale M P 1986 *Phys. Rev. Lett.* **56** 742
[14] Nienhuis B 1989 to be published
[15] Izergin A G and Korepin V E 1981 *Commun. Math. Phys.* **79** 303
[16] Vichirko V I and Reshetikhin N Yu 1983 *Theor. Math. Phys.* (*USA*) **56** 805 (transl. from *Teor. Mat. Fiz.* (*USSR*) **56** 260)
[17] Affleck I 1986 *Phys. Rev. Lett.* **56** 746
[18] Cardy J L 1984 *J. Phys. A: Math. Gen.* **17** L385
[19] Blöte H W J, Nightingale M P and Derrida B 1981 *J. Phys. A: Math. Gen.* **14** L45
[20] Blöte H W J and Nightingale M P 1982 *Physica* **112A** 405
[21] Blöte H W J and Nightingale M P 1984 *Physica* **129A** 1
[22] Fan C and Wu F Y 1970 *Phys. Rev.* B **2** 723
[23] den Nijs M P M 1985 *Phys. Rev.* B **32** 4785
[24] Rommelse K and den Nijs M P M 1987 *Phys. Rev. Lett.* **59** 2578
[25] Teitel S and Jayaprakash C 1983 *Phys. Rev.* B **27** 598
[26] Thijssen J M and Knops H J F 1988 *Phys. Rev.* B **38** 9080
[27] Foda O 1988 *Nucl. Phys.* B **300** 611
[28] Duplantier B and Saleur H 1987 *Nucl. Phys.* B **290** 291
[29] van Leeuwen J M J 1975 *Phys. Rev. Lett.* **34** 1056
[30] Nienhuis B and Nauenberg M 1976 *Phys. Rev.* B **13** 2021
[31] Baxter R J 1972 *Ann Phys.* **70** 193
[32] Baxter R J, Kelland S B and Wu F Y 1976 *J. Phys. A: Math. Gen.* **9** 397
[33] Zamolodchikov A B and Fateev V A 1980 *Sov. J. Nucl. Phys.* **32** 298 (transl. from *Yad. Fiz.* (*USSR*) **32** 581)
[34] Alcaraz F C and Martins M J 1988 *Phys. Rev. Lett.* **61** 1529
[35] Affleck I 1986 *Nucl. Phys.* B **265** 409
[36] Baxter R J 1973 *J. Phys. C: Solid State Phys.* **6** L455
[37] Barber M N and Batchelor M T 1989 *Preprint*